Trapped pore waters in the open proton channel H_V1

Danila Boytsov[1,†] , Stefania Brescia[1,†], Gustavo Chaves[2], Christof Hannesschlaeger[1], Christine Siligan[1], Nikolaus Gössweiner-Mohr[1], Boris Musset[2], Peter Pohl[1,*]

[1]Institute of Biophysics, Johannes Kepler University, 4020 Linz, Gruberstr. 40, Austria
[2]Institute of Physiology, Pathophysiology and Biophysics, CPPB, Paracelsus Medical University, Nuremberg, Germany

† These authors contributed equally to the paper
* Correspondence to: peter.pohl@jku.at

Abstract

The voltage-gated proton channel, H_V1, is crucial for innate immune responses. According to alternative hypotheses, protons either hop on top of an uninterrupted water wire or bypass titratable amino acids, interrupting the water wire halfway across the membrane. To distinguish between both hypotheses, we estimate the water mobility for the putative case of an uninterrupted wire. The predicted single-channel water permeability $\approx 10^{-12} cm^3 s^{-1}$ reflects the permeability-governing number of hydrogen bonds between water molecules in single-file configuration and pore residues. However, the measured unitary water permeability does not confirm the prediction, i.e., it is negligible. Osmotic deflation of reconstituted lipid vesicles reveals trapped water inside the H_V1 wild-type channel and D174A mutant open at 0 mV. At least one intervening amino acid acts as a barrier to water flow in the open channel while allowing protons to pass.

Introduction

The voltage-gated proton channel H_V1 is expressed in discrete cell types (*1*). Among other roles, it is involved in innate immunity (*2*) - its primary function being the acid extrusion from cells. Both transmembrane voltage and the transmembrane pH gradient gate H_V1 (*3*). Its structure is homologous to classical voltage-gated channels' voltage-sensing domain (VSD) (*4*). Experimentally, exclusively closed structures are available –a crystal structure of a chimera between mouse H_V1 and Ciona intestinalis voltage-sensing phosphatase (*5*) and an NMR structure of the human H_V1 (*6*). Also, electron paramagnetic resonance (EPR) spectroscopy data decipher the resting structure of H_V1 (*7*). The open channel's structure has solely been computed as homology models (*8-14*). Therefore, the molecular mechanism of proton transfer is still debated (*15, 16*).

The first hypothesis of proton permeation stipulates that charged residues interrupt the H_V1 spanning water wire, i.e., water molecules are trapped inside the H_V1 channel (*10*). In contrast to water, protons can still traverse the channel by hopping from one acidic residue to the next through a bridging water molecule (*11*) or, vice versa, by hopping along water wires linked by titratable residues (*17, 18*).

According to the second hypothesis, protons move through the open H_V1 by hopping over an uninterrupted file of water molecules (*19*), i.e., the same way they move through the peptide channel gramicidin A (*20*), via Grotthuss' mechanism (*21*). Molecular dynamics simulations based on the $K_v1.2$–$K_v2.1$ paddle-chimera VSD support the view by showing an uninterrupted water wire that extends through the membrane (*9*).

Significantly, the intraluminal water molecules must arrange in a single file, i.e., the pore is so narrow that the molecules cannot overtake each other (Fig. 1). Other physiologically essential channels may harbor water molecules similarly: gramicidin, aquaporins, and potassium-selective channels (*22*). All of them facilitate water transport (*23*). The rate at which water crosses these single-file channels can be predicted from the number, N_H, of hydrogen bonds that the molecules may form with pore-lining residues (*24, 25*). The larger N_H, the smaller the unitary water permeability p_f. H_V1 offers 12 residues, which may form hydrogen bonds with pore waters (Fig. 1). N_H of human aquaporin-1 or bacterial aquaporin-Z is equal in size (*24*). Consequently, H_V1's p_f should adopt a value of the same order of magnitude. This observation paves the way for investigating the second hypothesis experimentally by measuring the mobility of H_V1's water wire.

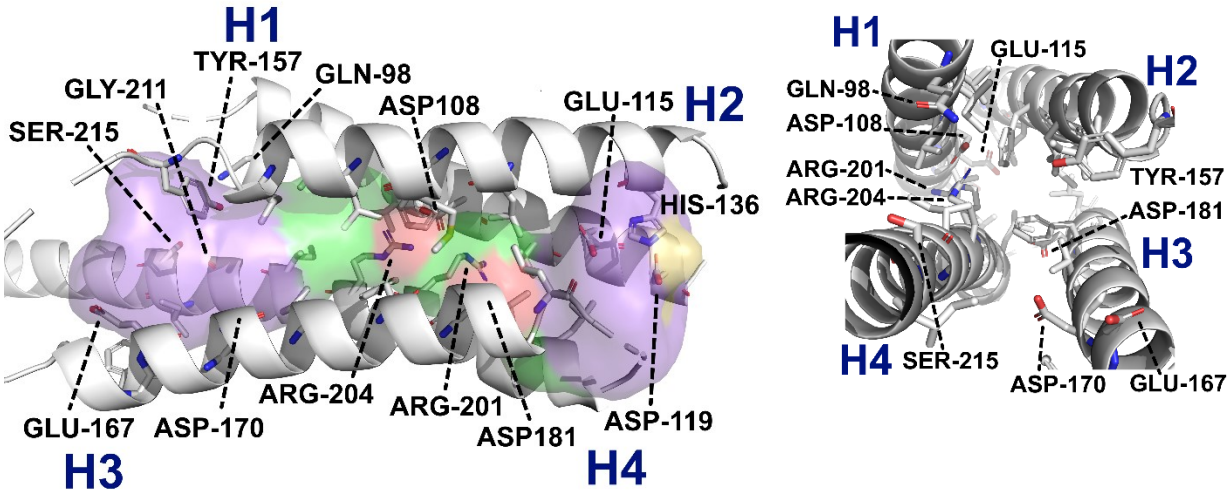

Fig. 1. Structure of the closed H_V1 **channel** (*Mus musculus*, PDB: 3WKV, 10.1038/nsmb.2783). (A) Line of 12 potential H-bond donors and acceptors guiding water through the H_V1 pore from the cytoplasm (left) to the periplasm (right). Phe157 has been changed to Tyr in 3WKV and thus does not contribute to H-bond interactions in wild type H_V1. In 3WKV, the backbone oxygen of Gly211 faces the channel and does not form the usual helix-internal connection to the backbone nitrogen of Ser215. We generated the pore surface with the program HOLE (*26*): Green areas represent pore radii suitable for a single water molecule only, red colored pore surfaces are too narrow to let water molecules pass, and purple regions can accommodate more than one water molecule per cross section. (B) View along the channel (cyto > peri).

Results

We aimed to perform the water flux measurements in a reconstituted system to answer whether the water molecules in H_V1 are trapped unambiguously. This experimental design requires the channel to be in its open configuration at zero transmembrane potential. Previous experiments suggest that the D174A mutant meets the requirement (*19*). We confirmed the observation by performing patch-clamp studies in whole-cell configuration and comparing D174A to wild-type H_V1 (Fig.2).

Whole-cell patch-clamp

We overexpressed wild-type H_V1 and the H_V1 D174A in tsa 201 cells. We found a threshold potential around – 70 mV (Fig. 2A) in symmetrical pH conditions using our previously

published protocol (*27, 28*). In contrast, the wild type is mainly closed at 0 mV which is its threshold potential (Fig. 2B). At the same time, the D174A mutant retains nearly perfect proton selectivity, i.e., the measured reversal potential was close to the Nernst potential for protons (Fig. 2C). Repeated experiments at different pHs showed that the threshold potential of the mutant is always more negative than the reversal potential for protons.

Consequently, the mutant channel is nearly fully open without external voltage (Fig. 2D), readily seen in the tail current amplitude reaching a quasi-saturation (Fig. 2A). Interestingly, the conductance density mediated by the expression of the mutant was 2.5 times smaller than the wild type, although we transfected the same amount of plasmid DNA (Fig. 2E). Assuming that protein expression is independent of the mutation, the observation suggested that the unitary proton flux ratio R_C of wild type to mutant channel was equal to 2.5. Furthermore, the resulting outward currents have a higher amplitude in the wild-type (Fig. 2A+B). The conductance density relationship (Fig. 2E) compares the maximal conduction of both constructs; this is the fully open channel (open probability ≈ 1). Thus, D174A, while opening with less depolarization, conducts protons at a lower rate.

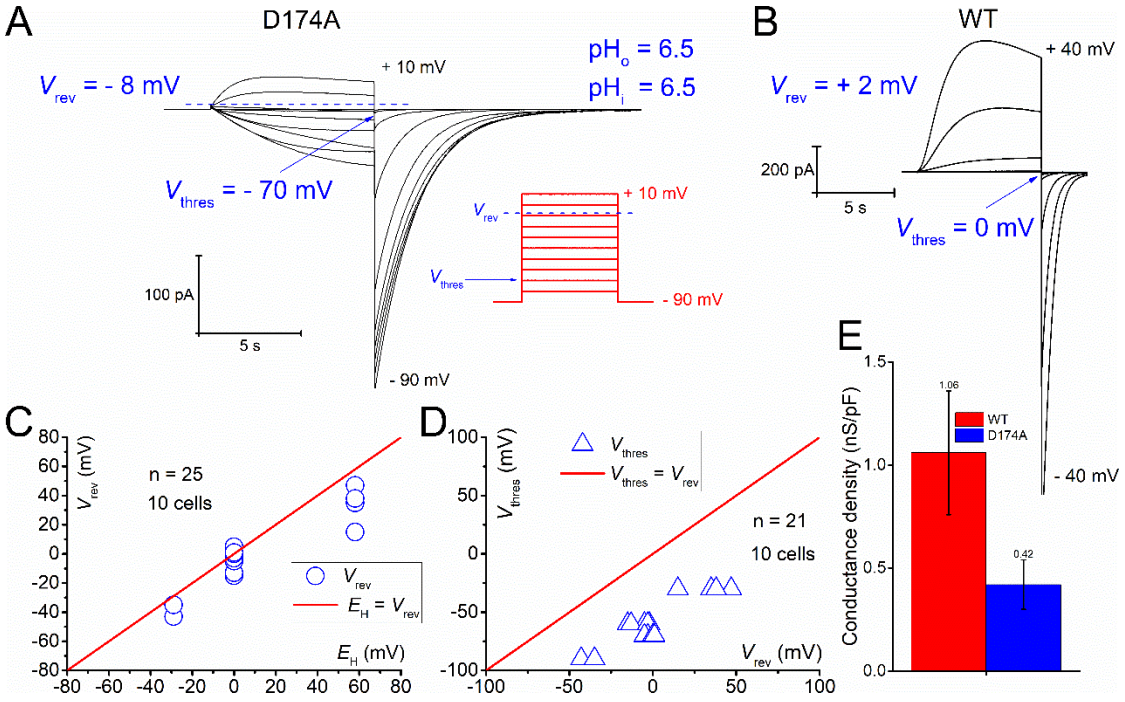

Fig. 2. Typical whole-cell patch-clamp measurement of human H_V1 D174A mutant in tSA201 cells. **(A)** Family of proton currents due to depolarizing pulses from – 90 mV to + 10 mV, in 10 mV increments, at pH_o 6.5 and pH_i 6.5. Pronounced inward H^+ currents activate negatively to reversal potential (here – 70 mV), indicating a high open probability of the D174A mutant at 0

mV. **(B)** Wild type H_V1 activates close to the reversal potential and depicts a low open probability at 0 mV. **(C)** Comparison of calculated Nernst potential for protons (E_H) and measured reversal potential (V_{rev}). The red line indicates perfect proton selectivity. **(D)** Comparison of the threshold of activation (V_{thres}) and measured reversal potential (V_{rev}) for the D174A mutant, indicating a high open probability without application of external voltage. **(E)** Comparison of the conductance density of cells expressing wild-type H_V1 and D174A mutant.

Our experiments with the purified and reconstituted channels corroborated the conclusion (Fig. 3A). The ratio R of the proton flux rate $\lambda_{D,wt}$ per wild type dimer and the flux rate $\lambda_{D,D174A}$ per mutant dimer was equal to: $R_f = \frac{\lambda_{D,wt}}{\lambda_{D,D174A}} = \frac{0.41}{0.17} = 2.4$ (Fig. 3B).

To obtain λ_D, we encapsulated 150 mM KCl into the H_V1 containing large unilamellar vesicles (LUVs) and exposed these vesicles to a buffer, where we substituted KCl for NaCl. The addition of valinomycin facilitated K^+ efflux, thereby inducing a membrane potential, ψ. ψ constituted the driving force for H^+ uptake. To assess the uptake rate, we measured the fluorescence of the weak acid 9-amino-6-chloro-2-methoxyacridine (ACMA). It is freely permeable across the vesicle membrane (*29*). Yet, when protonated, it becomes trapped in the LUVs, and the fluorescence intensity, I, decreases. The dimerization (or oligomerization) of protonated ACMA is most likely responsible (*30*). Fitting a monoexponential function to I(t) yielded λ. Plotting λ as a function of the number of dimers per vesicle (Fig. 3) allowed calculating the transport rate λ_D per dimer.

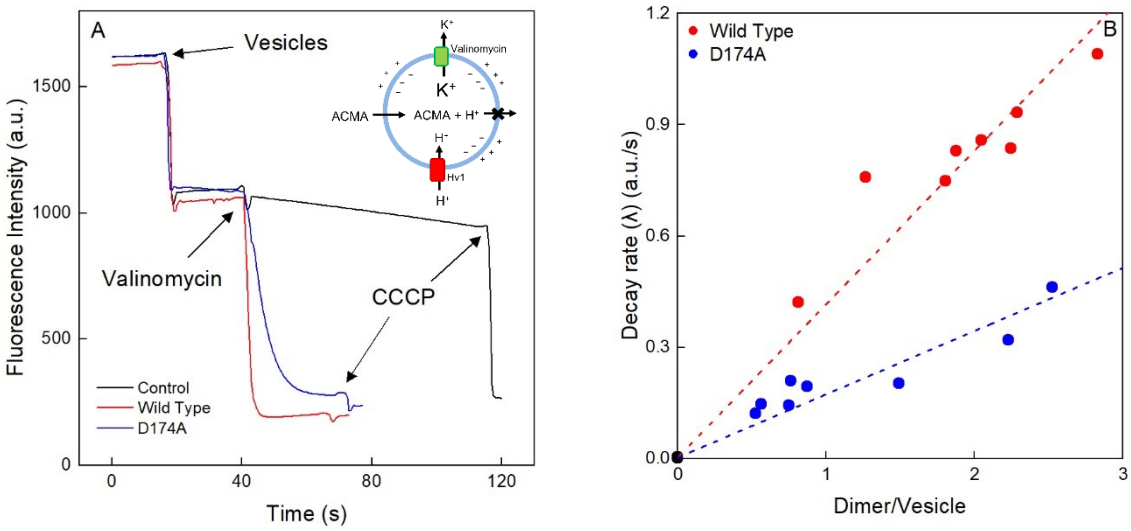

Figure 3. Representative records of the experiments used to assess vesicular acidification. A) The addition of vesicles to the dye (ACMA) containing buffer led to a decrease of the fluorescence intensity (I in a.u.) due to the (i) dilution and (ii) uptake of the dye into the vesicles. The

subsequent addition of valinomycin facilitated K^+ efflux, which in turn gave rise to the formation of membrane potential. The latter induced proton uptake via wild-type Hv1 (red) or the D174A mutant (blue), accompanied by a pronounced fluorescence decrease. The background permeability of the lipid bilayers to protons was much smaller, as indicated by the moderate fluorescence intensity change detected for control vesicles (black). The addition of carbonyl cyanide m-chlorophenyl hydrazone (*CCCP*) revealed the relative size of the vesicle population without Hv1. The temperature was equal to 23 °C. Inset: Schematic illustration of the fluorescence-based H^+ flux assay: 150 mM KCl inside the vesicles, 150 mM NaCl outside. B) Proton uptake rate, λ, as a function of protein abundance in the membrane. A linear fit to the data measured for the wild type Hv1 (red) and the D174A mutant (blue) yielded the dashed lines. Their slopes indicate a rate $\lambda_D = (0.41 \pm 0.019)$ a.u.s^{-1} per wild type dimer and $\lambda_D = (0.17 \pm 0.013)$ a.u.s^{-1} per mutant dimer. λ for empty vesicles amounted to $\lambda = 0.00196$ s^{-1} (black). λ was determined by fitting a monoexponential function to the *I*=f(time) traces (see panel A). We performed three independent purifications and reconstitutions for each wild type and mutant to obtain λ.

Fluorescence correlation spectroscopy (FCS) revealed the number of dimers per vesicle (*31*). Therefore, FCS first counted the number N_{PL} of proteoliposomes per confocal volume. Subsequently, a mild detergent (octyl glucoside) dissolved the LUVs and FCS counted the number N_{MD} of dimer-containing micelles. Taking the dilution into account, the ratio N_{PL}/N_{MD} yielded the number of dimers per vesicle. The subsequent addition of 3 M urea doubled the number of particles, indicating the dissolution of dimers into monomers (Suppl. Fig. 3).

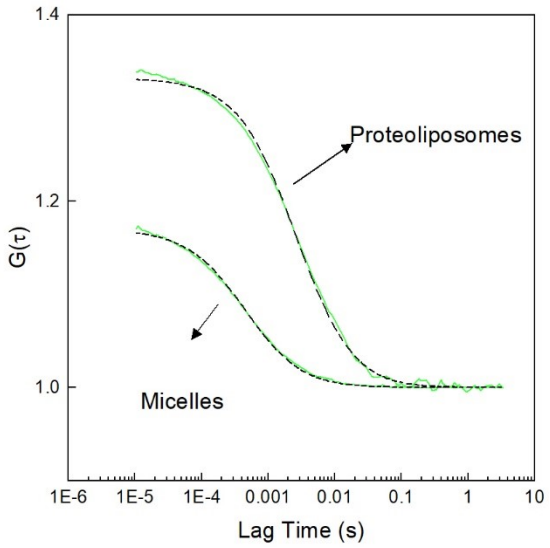

Figure 4. Representative autocorrelation curves $G(\tau)$ for the determination of reconstitution efficiency. Intensity fluctuations recorded by fluorescence correlation spectroscopy allowed G(τ) calculation. In turn, $G(\tau)$ served to determine the number $N_{PL} = 3.0$ of proteoliposomes and the number $N_{MD} = 5.9$ of micelles formed per confocal volume after the detergent's addition. After correcting the dilution during detergent addition, we found the number of dimers per vesicle $N_{PL}/N_{MD} = 2.25$.

LUVs with functionally reconstituted H_V1 and known channel numbers were subjected to an osmotic gradient in a stopped-flow device. We measured the intensity of scattered light *I* to follow the deflation kinetics (Fig. 5). However, both the proteoliposomes containing the wild type and the mutant channel did not show an increased water permeability, P_f, at room temperature (Suppl. Fig. 1). This result was independent of the number of reconstituted channels per vesicle. Considering the stark dependence of the activation energy for water flow across lipid bilayers (*25*), we repeated the experiments at a decreased temperature of 4°C. Since the activation energy for water flow through single file membrane channels weakly depends on temperature (*25*), we aimed at detecting tiny increments in water flow mediated by the channels. Yet, the channels did not contribute to the water flow through the vesicular membrane under these conditions. Both mutant and wild-type channels were still active at the decreased temperature, as demonstrated by the repetition of the proton flow experiments (Suppl. Fig. 2). A roughly twofold activity decrease accompanied the temperature drop of about 19°C.

The difference in measures transport rates allows a rough estimation of the Arrhenius activation energy E_a for H_V1-mediated proton flow. It amounts to 40 kJ/mol for the wild type and 23 kJ for the mutant. Thus, E_a exceeds the corresponding 15 kJ/mol barrier measured for gramicidin A (*32, 33*). The increment in E_a suggests that the transport mechanism may be different from a pure Grotthuss type, where the proton uses an uninterrupted water wire to cross the membrane.

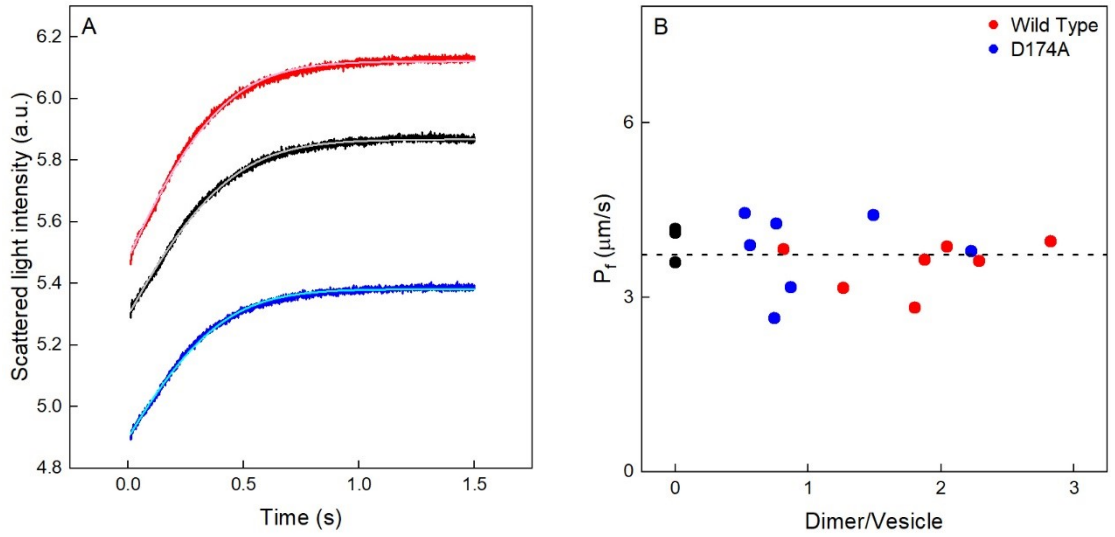

Figure 5. Water permeability of H_V1 containing LUVs. A) Representative shrinking curves of control vesicles (black curve), LUVs containing the D174A mutant (blue), or the wild type (red).

We fitted Equation 3 to the experimental data (grey, light blue, and pink curves) to calculate the vesicular water permeabilities P_f. It amounted to roughly 3.7 μm/s in all three cases. The proteoliposomes contained 0.56 and 0.8 dimers per vesicle. B). Repeating the experiments for different reconstitution levels showed no significant P_f difference between control (filled black circles) and reconstituted LUVs.

Discussion

Water molecules inside the H_V1 pore appear to be trapped. They serve as proton railways, as demonstrated by the vesicular proton uptake rate increment upon channel reconstitution. At the same time, they do not respond to an osmotic driving force, as indicated by the inability of the H_V1 mutant D174A open at 0 mV to facilitate water transport across the vesicular membrane.

The observation rules out the formation of an uninterrupted water chain spanning the open channel from the aqueous solution at one side of the membrane to the other. N_H would have governed water mobility if such a water wire had formed (*24*). Specifically, every H-bond donating or receiving pore-lining residue would have contributed an increment $\Delta\Delta G^{\ddagger}$ of 0.1 kcal/mol to the Gibbs free energy of activation $\Delta G^{\ddagger}$ (*25*). Equation (1) allows the calculation of $\Delta G^{\ddagger}$:

$$\Delta G^{\ddagger} = N_H \, \Delta\Delta G^{\ddagger} + \Delta\Delta G_{\mathrm{i}}^{\ddagger} \tag{1}$$

where $\Delta G^{\ddagger}(N_{\mathrm{H}} = 0) = \Delta\Delta G_{\mathrm{i}}^{\ddagger} = 2$ kcal/mol (*25*). Since $N_{\mathrm{H}} = 12$ (Fig. 1) in H_V1, Eq. 1 predicts $\Delta G^{\ddagger} = 3.2$ kcal/mol. Eq. (2) allows calculating H_V1's unitary water permeability p_f from this value (*34*):

$$p_{\mathrm{f}} = \nu_0 v_{\mathrm{w}} \cdot \exp(-\Delta G^{\ddagger}/\mathrm{R}T) \tag{2}$$

where $v_w = 3 \times 10^{-23}$ cm^3 is the volume of one water molecule and ν_0 is the universal attempt frequency, $\nu_0 = k_B \cdot T/h \approx 8.2 \times 10^{12}$ s^{-1} at room temperature (k_B is Boltzmann's and h is Planck's constant). With $p_f = 1.1 \times 10^{-12}$ cm^{3}s^{-1}, a single H_V1 dimer would have contributed $2 \times p_f/A = 2.2 \times 10^{-12}$ cm^{3}s^{-1}/(4 π (50 nm)^2) = 71 μm s^{-1} to vesicle P_f, where A is the surface area of the vesicle. That is, upon reconstitution of a single dimer, vesicle P_f should have doubled at room temperature and increased by one order of magnitude at 4°C. We did not observe the predicted changes (Fig. 5).

This result indicates that pore residues interrupt the H_V1 spanning water wire, trapping the water molecules inside the H_V1 channel. In contrast to water, protons cross the pore by

163 hopping from one acidic residue to another through one or more bridging water molecules
164 (Fig. 6).
165

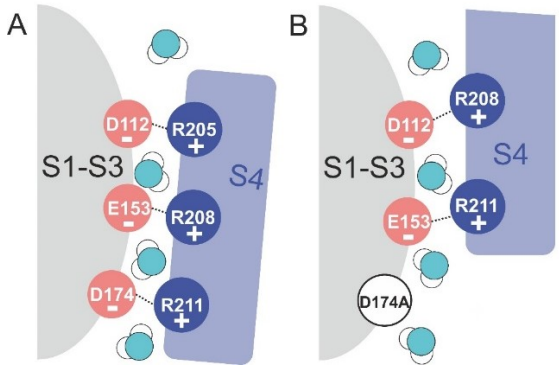

Figure 6. Simplified scheme of proton transport with trapped water molecules inside the channel. A) The resting wild-type channel. Black dashed lines represent the salt bridges between titratable residues from S1-S3 with residues from S4. B) Removal of D174 of S3 abolishes its salt bridge with R211 from S4. Instead, R211 forms a salt bridge with E153, i.e., the channel opens without transmembrane voltage. Now, residue R208 forms the salt bridge with the D112 residue, allowing protons to pass (*7, 10*). Cyan spheres represent water molecules, light red circles stand for the negatively charged residues, and light blue residues depict positively charged arginine residues on the S4 subunit.

166
167 The threshold potential to reversal potential relationship is one of the hallmarks of the
168 voltage-gated proton channel Hv1 (*35, 36*). Here we characterized the shift of the voltage
169 dependence in the D174A mutant and the resulting negative threshold potential (Fig.2
170 C+D). Drastically prolonged tail current kinetics might reflect a decreased voltage
171 dependence of the deactivation in the D174A mutant. The observation suggests that D174
172 stabilizes the closed state, i.e., its elimination reduces the number of hydrogen bonds
173 favoring the closed conformation (*14*). The potential involvement of D174 in the proton
174 permeation pathway provides an alternative explanation (*12*). Removal of the negatively
175 charged entrance point to the pore must reduce conductivity. This scenario is in line with
176 the 2.5-fold decreased proton flux through mutant observed in both current and fluorescence
177 measurements.
178

Materials and Methods

Experimental Design

First, we looked for an H_V1 mutant with a high open probability at zero transmembrane potential. We performed whole-cell recordings of overexpressed human H_V1 wild type and the D174A mutant.

We assessed H_V1's water-conducting ability in a reconstituted system. That is, we purified the overexpressed human H_V1 channel from insect cells and reconstituted it into large unilamellar vesicles (LUVs). H_V1 facilitated proton transport as judged by intravesicular pH changes in response to the application of transmembrane potential. Recording the intensity of scattered light allowed quantifying the osmotically induced vesicle deflation.

Heterologous expression in mammalian cells and electrophysiology

H_V1-wild type and D174A mutant DNA were synthesized (Eurofins/Genomics, Ebersberg, Germany) and cloned into a pEX-A2 using 5′ *Bam*HI and 3′ *Eco*RI restriction sites. Constructs were later sub-cloned into a pQBI25-fC3 or pcDNA3.1, using 5′*Bam*HI and 3′ *Eco*RI restriction sites and GFP fused to N-terminal (*27, 28*).

tSA201 cells (human kidney cell line) were cultivated to 85% confluency in 35 mm culture dishes and transfected with 1.0 µg plasmid DNA using polyethyleneimine (Sigma, St. Louis, MO, USA). After 12 h at 37 °C in 5% CO_2, cells were trypsinized and replated onto glass coverslips at low density for patch-clamp recordings and measurements done between 2 – 12 hours afterward. We selected cells emitting green fluorescence. The expression level for wild-type and D174A mutant allowed discarding the contamination of native proton channels. Whole-cell patch-clamp measurements showed no other voltage- and time-dependent conductance at recording conditions.

Whole-cell patch-clamp recordings (HEKA EPC 10, Lambrecht, Germany) were stored on hard discs and analyzed with ORIGIN® (OriginLab, Northampton, MA, USA). Pipettes were pulled from borosilicate capillaries GC 150TF-10 (Harvard Apparatus, Holliston, MA, USA). tetramethylammonium (TMA^+) and methanesulfonate ($CH_3SO_3^-$) constituted the main ions in the whole-cell solutions (pipette and bath) in a concentration range of 90 - 125 mM. We also added 1 mM EGTA, 1 mM Mg^{2+} and 100 mM of a buffer with a pKa close to pH: 2-(N-morpholino)ethanesulfonic acid (MES) at pH 5.5, Bis(2-hydroxyethyl)amino-tris(hydroxymethyl)methane (BIS-TRIS) at pH 6.5 and N,N-bis(2-hydroxyethyl)-2-aminoethanesulfonic acid (BES) at 7.0. Seals were usually > 3 GΩ. Currents are shown without any correction for the leak or liquid junction potentials. We collected the data

213 between 18 to 21 °C. Two methods determined reversal potentials (V_{rev}): when the
214 threshold of activation (V_{thres}) was negative to V_{rev} it was determined by the zero current,
215 while when V_{thres} was positive to V_{rev}, then V_{rev} was determined with the tail current method

216 *Purification of* H_V1

217 The H_V1 wild type and mutant D174A were expressed as an N-terminal 10×His-GFP fusion
218 HVCN1 gene in Tni PRO cells (ProTech service, VBCF Protein Technologies Facility,
219 Vienna BioCenter, Vienna, Austria). At 20000 psi, an EmulsiFlex-C5 homogenizer
220 (Avestin, Inc., Ottawa, ON, Canada) disrupted the resuspended cell pellet in a buffer
221 containing 150 mM Tris-HCl (pH 8.0), 500 mM NaCl, and a cocktail of proteinase
222 inhibitors (Roche, Basel, Switzerland). Centrifugation for 10 minutes at 7000xg (4°C)
223 pelleted the dell debris. 3 M Urea and 5 mM β-mercaptoethanol stripped the membranes
224 within 2 hours at 4°C. Overnight, 1.5% DDM (Anatrace, Inc., Maumee, OH, USA)
225 dissolved the resuspended membrane pellet obtained by ultracentrifugation for 1 hour at
226 100,000 × g (4°C). 30 minutes of centrifugation at 30000 × g yielded the supernatant
227 subsequently subjected to affinity purification by Ni-NTA resin (Cube Biotech GmbH,
228 Monheim am Rhein, Germany). A washing step with a buffer containing 150 mM Tris-HCl
229 (pH 7.5), 500 mM NaCl, 0.5% DDM, 80 mM imidazole, and proteinase inhibitor cocktail
230 followed 2 h of incubation at 4°C on an over-head shaker (Sunlab Tube roller D-8400,
231 neoLab Migge GmbH, Heidelberg, Germany). The elution buffer contained an additional
232 0.5 M imidazole. An SDS-PAGE documented H_V1 purity. Fluorescence correlation
233 spectroscopy (FCS) determined protein concentration.

234

235 *Reconstitution of* H_V1

236 A buffer containing 150 mM KCl, 5 mM HEPES (pH 7.5), EGTA 0.5 mM hydrated a dry
237 lipid film preformed from *E. coli* polar lipid extract (Avanti Polar Lipids, Inc., Alabaster,
238 AL, USA) on the walls of a flask. An ultrasonication bath (Avanti Polar Lipids, Inc.,
239 Alabaster, AL, USA) increased the transparency of the 20 mg/ml lipid solution. 40 mM DM
240 primed the lipid mixture for the sequential addition of the H_V1 detergent mixture. 72 hours
241 of dialysis with tubings containing 15 kDa cutoff pores and subsequent ultracentrifugation
242 (Optima LE-80K, Beckman Coulter Ultracentrifuge, Beckman Coulter Inc., Brea, CA,
243 USA) at 100,000 × g for 2 hours at 4°C removed the detergent. Extrusion through 100 nm
244 pore size filters of the resuspended proteoliposomes yielded uniformly sized large
245 unilamellar vesicles.

246

247 *Fluorescence correlation spectroscopy (FCS)*

248 We used FCS to estimate H_V1 abundance in reconstituted vesicles (*37*). In brief, the FCS
249 unit (Confocor3, Carl Zeiss, Jena, Germany) of a commercial laser scanning microscope
250 (LSM 510) measured the temporal fluctuations of the fluorescence intensity I in the focal
251 volume of a C-Apochromat 40x/1.2W objective. The corresponding autocorrelation
252 function $G(\tau)$ yielded (i) the average number $\langle N \rangle$ of protein-containing particles in the focal
253 volume of radius r and elongation z of the focus in the direction of the laser beam, and (ii)
254 their diffusion coefficient D_v (*38*):

255 $$G(\tau) = \frac{1}{\langle N \rangle}\left[1 + \frac{4D_v\tau}{r^2}\right]^{-1}\left[1 + \frac{4D_v\tau}{z^2}\right]^{-\frac{1}{2}} \quad (3)$$

256 Dissolving the LUVs in mild detergent yielded protein-containing micelles. The ratio of
257 micelles to LUVs indicated the number of dimers per vesicle. Using urea allowed for
258 determining the number of monomers per LUV.

259

260 *Proton uptake into LUVs*

261 Transmembrane voltage constituted the driving force for proton uptake into LUVs (Figure
262 M). It resulted from facilitated K^+ efflux out of the vesicles (*30*). The ensuing vesicular
263 acidification led to the protonation of the dye 9-Amino-6-chloro-2-methoxyacridine
264 (ACMA). Yet the intravesicular concentration of the unprotonated form did not change
265 since it is a weak base that can freely move across the membrane in its neutral form.
266 Intravesicular accumulation of ACMA's protonated form decreased detectable fluorescence
267 – conceivably due to dye dimerization (*39*).

268 The extravesicular buffer contained 5 mM HEPES (pH 7.5), 150 mM NaCl, 0.2 mM EGTA
269 and 2 µM ACMA. Sample excitation at 275 nm and measurements of the resulting
270 fluorescence at 475 nm (Fluorescence Spectrophotometer F-2700, Hitachi, Ltd., Chiyoda
271 City, Tokyo, Japan) under vigorous stirring and temperature control (set to 23°C or 4°C)
272 allowed time-lapse experiments. They started with the addition of 25 µl of a LUV
273 suspension (10 mg lipid per ml), followed by pipetting 0.5 µl DMSO solution containing 1
274 mM valinomycin. Additions of 1.5 µM carbonyl cyanide m-chlorophenyl hydrazone
275 (CCCP) equilibrated pH at the end of the experiment.

276

277

Water efflux measurements

Water efflux leads to a decrease of vesicle volume V. The latter can be accessed via measurements of the intensity *I* of scattered light at a wavelength of 480 nm (*24*) according to Equation 3:

$$I(t) = a + b[V(t)] + d[V(t)]^2 \quad (4)$$

where the parameters *a, b,* and *d* are fitting parameters. We found *a* from Equation (5):

$$a = I(\infty) - bV_f - dV_f^2 \;;\; where \;\; V_f = V_0 c_0^i/(c_0^i + c_S) \quad (5).$$

c_0^i and c_s are the initial osmolyte concentrations inside the vesicles and the incremental osmolyte concentration in the external solution, respectively. The rate of the osmotically driven volume decrease determines the vesicular water permeability P_f (Equation 6):

$$V(t) = V_0 \frac{c_0^i}{c_0^i + c_S}\left\{1 + L\left(\frac{c_S}{c_i^0} exp\left(\frac{c_S}{c_0^i} - \frac{AP_f V_w (c_0^i + c_S)^2}{V_0 c_0^i} t\right)\right)\right\} \quad (6)$$

where V_w, V_0, and L are the molar volume of water, vesicle volume at time zero, and the Lambert function: $L(x)e^{L(x)} = x$, respectively {Horner, 2015 #6785}.

The system of Equations (4-6) was globally fitted to the whole set of shrinking curves obtained in a stopped-flow device (SFM 3000, Bio-Logic, Seyssinet-Pariset, France) from a particular reconstitution sample to extract the fitting parameters *b*, *d*, and *P*.

References

1. T. E. DeCoursey, Voltage-gated proton channels: molecular biology, physiology, and pathophysiology of the H(V) family. *Physiol. Rev.* **93**, 599-652 (2013).
2. E. Montes-Cobos *et al.*, Voltage-Gated Proton Channel Hv1 Controls TLR9 Activation in Plasmacytoid Dendritic Cells. *The Journal of Immunology* **205**, 3001 (2020).
3. T. E. DeCoursey, Voltage and pH sensing by the voltage-gated proton channel, HV1. *J R Soc Interface* **15**, (2018).
4. F. Tombola, M. H. Ulbrich, E. Y. Isacoff, Architecture and gating of Hv1 proton channels. *J Physiol* **587**, 5325-5329 (2009).
5. K. Takeshita *et al.*, X-ray crystal structure of voltage-gated proton channel. *Nat. Struct. Mol. Biol.* **21**, 352-357 (2014).
6. M. Bayrhuber *et al.*, Nuclear magnetic resonance solution structure and functional behavior of the human proton channel. *Biochemistry* **58**, 4017-4027 (2019).
7. Q. Li *et al.*, Resting state of the human proton channel dimer in a lipid bilayer. *Proc Natl Acad Sci U S A* **112**, E5926-5935 (2015).
8. J. A. Freites, D. J. Tobias, S. H. White, A voltage-sensor water pore. *Biophys. J.* **91**, L90-92 (2006).
9. M. L. Wood *et al.*, Water wires in atomistic models of the Hv1 proton channel. *Biochim Biophys Acta* **1818**, 286-293 (2012).
10. K. Kulleperuma *et al.*, Construction and validation of a homology model of the human voltage-gated proton channel hHV1. *J. Gen. Physiol.* **141**, 445-465 (2013).

11. S. C. van Keulen *et al.*, Does Proton Conduction in the Voltage-Gated H+ Channel hHv1 Involve Grotthuss-Like Hopping via Acidic Residues? *The Journal of Physical Chemistry B*, (2016).
12. R. Banh *et al.*, Hydrophobic gasket mutation produces gating pore currents in closed human voltage-gated proton channels. *Proc Natl Acad Sci U S A* **116**, 18951-18961 (2019).
13. A. D. Geragotelis *et al.*, Voltage-dependent structural models of the human Hv1 proton channel from long-timescale molecular dynamics simulations. *Proc Natl Acad Sci U S A* **117**, 13490-13498 (2020).
14. C. Jardin, N. Ohlwein, A. Franzen, G. Chaves, B. Musset, The pH-dependent gating of the human voltage-gated proton channel from computational simulations. *Phys. Chem. Chem. Phys.*, 10.1039/d1031cp05609c (2022).
15. T. E. DeCoursey, CrossTalk proposal: Proton permeation through HV1 requires transient protonation of a conserved aspartate in the S1 transmembrane helix. *The Journal of Physiology* **595**, 6793-6795 (2017).
16. A. L. Bennett, I. S. Ramsey, CrossTalk opposing view: proton transfer in Hv1 utilizes a water wire, and does not require transient protonation of a conserved aspartate in the S1 transmembrane helix. *The Journal of physiology* **595**, 6797-6799 (2017).
17. E. Gianti, L. Delemotte, M. L. Klein, V. Carnevale, On the role of water density fluctuations in the inhibition of a proton channel. *Proceedings of the National Academy of Sciences* **113**, E8359-E8368 (2016).
18. M. Lee, C. Bai, M. Feliks, R. Alhadeff, A. Warshel, On the control of the proton current in the voltage-gated proton channel Hv1. *Proceedings of the National Academy of Sciences* **115**, 10321-10326 (2018).
19. I. S. Ramsey *et al.*, An aqueous H+ permeation pathway in the voltage-gated proton channel Hv1. *Nat. Struct. Mol. Biol.* **17**, 869-875 (2010).
20. R. Pomes, B. Roux, Molecular Mechanism of H+ Conduction in the Single-File Water Chain of the Gramicidin Channel. *Biophys. J.* **82**, 2304-2316 (2002).
21. N. Agmon *et al.*, Protons and hydroxide ions in aqueous systems. *Chem. Rev.* **116**, 7642-7672 (2016).
22. M.-C. Bellissent-Funel *et al.*, Water Determines the Structure and Dynamics of Proteins. *Chem. Rev.* **116**, 7673-7697 (2016).
23. A. Horner, P. Pohl, Single-file transport of water through membrane channels. *Faraday Discuss.* **209**, 9-33 (2018).
24. A. Horner *et al.*, The mobility of single-file water molecules is governed by the number of H-bonds they may form with channel-lining residues. *Science Advances* **1**, e1400083 (2015).
25. J. Pfeffermann, N. Goessweiner-Mohr, P. Pohl, The energetic barrier to single-file water flow through narrow channels. *Biophysical Reviews* **13**, 913-923 (2021).
26. O. S. Smart, J. G. Neduvelil, X. Wang, B. A. Wallace, M. S. P. Sansom, HOLE: A program for the analysis of the pore dimensions of ion channel structural models. *J. Mol. Graphics* **14**, 354-360 (1996).
27. G. Chaves, C. Derst, C. Jardin, A. Franzen, B. Musset, Voltage-gated proton channels in polyneopteran insects. *FEBS Open Bio* **12**, 523-537 (2022).
28. G. Chaves, S. Bungert-Plumke, A. Franzen, I. Mahorivska, B. Musset, Zinc modulation of proton currents in a new voltage-gated proton channel suggests a mechanism of inhibition. *FEBS J.* **287**, 4996-5018 (2020).
29. A. Marty, M. Bourdeaux, M. Dell'Amico, P. Viallet, 9-amino-2-methoxy-6-chloroacridine monocation fluorescence analysis by phase-modulation fluorometry. *Eur. Biophys. J.* **13**, 251-257 (1986).

30. S. Y. Lee, J. A. Letts, R. MacKinnon, Functional reconstitution of purified human Hv1 H+ channels. *J. Mol. Biol.* **387**, 1055-1060 (2009).
31. T. Hoomann, N. Jahnke, A. Horner, S. Keller, P. Pohl, Filter gate closure inhibits ion but not water transport through potassium channels. *Proc. Natl. Acad. Sci. U.S.A.* **110**, 10842-10847 (2013).
32. M. Akeson, D. W. Deamer, Proton conductance by the gramicidin water wire. Model for proton conductance in the F1F0 ATPases? *Biophys. J.* **60**, 101-109 (1991).
33. G. d. G. Marcelo, S. Cukierman, Modulation of Proton Transfer in the Water Wire of Dioxolane-Linked Gramicidin Channels by Lipid Membranes. *Biophys. J.* **81**, 1430-1438 (2001).
34. A. Horner, P. Pohl, Comment on "Enhanced water permeability and tunable ion selectivity in subnanometer carbon nanotube porins". *Science* **359**, (2018).
35. B. Musset *et al.*, Detailed comparison of expressed and native voltage-gated proton channel currents. *The Journal of physiology* **586**, 2477-2486 (2008).
36. T. E. DeCoursey, V. V. Cherny, Deuterium isotope effects on permeation and gating of proton channels in rat alveolar epithelium. *J Gen. Physiol* **109**, 415-434 (1997).
37. L. Erokhova, A. Horner, N. Ollinger, C. Siligan, P. Pohl, The Sodium Glucose Cotransporter SGLT1 Is an Extremely Efficient Facilitator of Passive Water Transport. *J. Biol. Chem.* **291**, 9712-9720 (2016).
38. E. L. Elson, D. Magde, Fluorescence correlation spectroscopy .1. Conceptual basis and theory. *Biopolymers* **13**, 1-27 (1974).
39. M. G. Palmgren, Acridine orange as a probe for measuring pH gradients across membranes: Mechanism and limitations. *Analytical Biochemistry* **192**, 316-321 (1991).

Acknowledgments

Funding:

This project has received funding from the European Union's Horizon 2020 research and innovation program under the Marie Skłodowska-Curie grant agreement No. 860592.

Author contributions:.

Conceptualization: BM, PP
Methodology: CS, CH
Investigation: DB, SB, GC
Visualization: SB, GC, NGM
Supervision: BM, PP
Writing—original draft: PP
Writing—review & editing: DB, SB, GC, CH, CS, NGM, BM, PP

Competing interests: Authors declare that they have no competing interests.

Data and materials availability: All data are available in the main text or the supplementary materials.